Acta Geologica Sinica (English Edition), 2019, 93(4): 928–942

Rare Earth Elements and Yttrium (REY) Geochemistry of Reefal Limestones in the Ordovician, Tarim Basin, NW China and their Paleoenvironment Implications

MENG Miaomiao[1, 2], LIU Xinxing[3, *], FAN Tailiang[2] and Ian J. DUNCAN[4]

[1] *Guangzhou Marine Geological Survey, China Geological Survey, Guangzhou 510760, China*
[2] *School of Energy Resources, China University of Geosciences, Beijing 100083, China*
[3] *School of Resources, Hebei GEO University, Shijiazhuang 050031, China*
[4] *Bureau of Economic Geology, The University of Texas at Austin, Austin, Texas 78758, USA*

Abstract: This study examines the rare earth elements and yttrium (REY) concentrations of twenty-five samples from the reef outcrop exposed along the Lianglitage Mountain in the Ordovician, Tarim Basin in China. The concentration analysis provides constraints on the paleoenvironment during reef deposition. Based on the detailed sedimentology and petrographic work, we divide the reef facies into four sub-facies: the base facies, reef-core facies, reef-flank facies, and sealing facies. The geochemical data (such as major and trace elements, carbon and oxygen isotopes, and REYs) are further used to study the coeval seawater characteristics as well as potential diagenesis overprints. The result indicated that the diagenesis has little effect on the REY patterns of the reefal limestones. The REY concentrations of the reefal limestones are overall low (ranging from 3.69 to 19.60 ppm, arithmetic mean=10.22 ppm, SD=5.4). The PAAS-normalized REY patterns are consistently flat compared to the typical well-oxidized, shallow marine water patterns. However, the light REE (LREE) depletions, positive La anomalies, negative Ce anomalies and positive Y anomalies, suggest that these reefal limestones are likely an indicative of contemporaneous seawater REY signals. The seawater-like Y/Ho ratios (average at 37.51) further support that REY signals in these limestones are likely a reflection of seawater with little diagenetic modifications. The low Y/Ho ratios presented only in the reef-flank facies and sealing facies are likely a suggestion of detrital contamination. Hence, this study confirms that REY patterns of the limestones at the base facies and reef-core facies can record ancient seawater information, and reefs can be used as a potential geochemical proxy for paleoenvironment studies throughout the Earth's history.

Key words: rare earth elements and yttrium (REY), limestones, depositional environment, Ordovician, Tarim Basin

Citation: Meng et al., 2019. Rare Earth Elements and Yttrium (REY) Geochemistry of Reefal Limestones in the Ordovician, Tarim Basin, NW China and their Paleoenvironment Implications. Acta Geologica Sinica (English Edition), 93(4): 928–942. DOI: 10.1111/1755-6724.13893

1 Introduction

The most significant factor controlling the rare earth elements (REE) chemistry of carbonate rocks is the composition of these elements dissolved in seawater (Elderfield et al., 1988; Piepgras and Jacobsen, 1992). REE signatures of ancient seawater reflect (1) the secular changes in the input source of REEs (Kamber and Webb, 2001; Kamber et al., 2004; Feng et al., 2009); (2) the variations in alkalinity and oxygenation levels of depositional environments (Greaves et al., 1999; Kim et al., 2012; Hu et al., 2014); and (3) paleobathymetry, oceanic circulation, paleogeography, and depositional environments (Kamber and Webb, 2001; Kemp and Trueman, 2003). In addition, REEs in carbonates can be useful to investigate the impact of diagenetic processes (Jiang et al., 2014 and 2015; Franchi et al., 2015).

REE compositions in carbonate are relatively stable and remain unaltered as long as the carbonate rocks have not undergone dissolution and recrystallization processes (Webb and Kamber, 2000; Shields and Webb, 2004; Azmy et al., 2011). Hence, the REE signatures in carbonates are regarded as proxies for paleoenvironment reconstructions in both Precambrian (Kamber and Webb, 2001; Allwood et al., 2007; Allwood et al., 2010) and Phanerozoic strata (Webb and Kamber, 2000; Nothdurft et al., 2004; Olivier and Boyet, 2006; Eltom et al., 2017).

REE characteristics of reefal limestones are good indicators of paleoenvironment conditions, such as the REE analyses of reefs during the Holocene (Webb and Kamber, 2000) and Devonian (Nothdurft et al., 2004), although there is an ongoing debate regarding the extent to which reefal limestones retain their original REE signatures. Foremost, concerns were largely focused on the potentials of diagenesis modifications (Webb and Kamber, 2000; Nothdurft, et al., 2004, Franchi et al., 2015). In this sense, any attempts to examine the possible impact on paleoenvironment of reefal limestones must first evaluate the diagenetic effect (Webb and Kamber, 2000).

In the Ordovician Tarim Basin, the REE analyses are seldom studied, and most of the published papers are about the study of diagenesis processes on the dolomite

* Corresponding author. E-mail: liuxinxing963@163.com

(Zhang et al., 2006; Han et al., 2009; Wang et al., 2009; Zhang et al., 2010; Zhang et al., 2014; Liu et al., 2017; Guo et al., 2018) and vein samples (Cai et al., 2008): however, the REY analysis of limestones is very limited. This motivates our study. The presented work is the first attempt to explore paleoenvironment based on the analyses of REE data from reefal limestones in the Ordovician Tarim Basin.

In this study, we collected a bunch of petrological and geochemical datasets (e.g., major and trace elements, REEs, carbon and oxygen isotopes) of reefal limestones in the Ordovician Tarim Basin. We use them to investigate the impact of diagenesis, redox, and terrestrial input on REY distributions of reefal limestones. Specifically, the tasks of this study are to (1) determine the REY patterns of different reefal-related facies; (2) evaluate the source of these REYs; (3) assess the possibility of using the REY patterns of the reefs as a paleoenvironment archive; (4) provide recommendations for future studies of REYs.

2 Geological Background

The Tarim Basin is the largest sedimentary basin in China, which is rich in oil and gas resources (Fig. 1a; Kang and Kang, 1996). The petroleum reservoirs are dominantly within the Ordovician strata, mainly consisting of shallow-water platform carbonates (Huang et al., 2017). The Tarim Basin is next to the Kunlun and Altun Mountains to the south, Tianshan Mountains to the north. It has an area of 560,000 km^2 (Fig. 1b). This basin, a peri-Gondwanan paleo-plate, was situated in the low to middle latitudes during the Ordovician (Huang et al., 2000; Torsvik and Cocks, 2013; Yang et al., 2017). During this period, reefs were developed worldwide (Webby, 2002), especially in the Ordovician Tarim Basin. The reef-related reservoirs in this basin are considered to be with high porosity and permeability. The reef complex occurs along the Lianglitage Mountain in the Yingshan and Yijianfang formations of the Lower-Middle Ordovician (Fig. 1c and 1d; Guo et al., 2010; Jiao et al., 2012; Li et al., 2017a).

The Yingshan Formation ($O_{1\text{-}2}y$, about 520 m thick) is characterized by grainstones, packstones, and dolostones (Fig. 1d). This formation was evolved from a restricted platform facies to an open platform facies. The Yijianfang Formation (O_2yj, about 70 m thick) is characterized by bioclastic grainstones and intraclastic grainstones that deposited in a platform margin setting (Fig. 1d; Gu et al., 2005).

3 Samples and Methods

3.1 Sample collections

A well-exposed reef in the Nanyigou profile (NYG reef) along the Lianglitage Mountain provides an outcrop that could possibly be used for studying the REY characteristics of reefal limestones. A total of twenty-five samples were carefully selected from the NYG reef (Fig. 2a). Four of them were collected from the base facies, two from the reef-core facies, five from the reef-flank facies, and fourteen from the sealing facies (Fig. 2b). When sampling, the following criteria were adopted to minimize potential contaminations: (1) siliciclastic materials, ferromanganese minerals, and phosphates were picked out as suggested by previous reseachers (Banner et al., 1988; Zhang, et al., 2008), (2) veins were ruled out, as they imply the diagenesis process, such as the influences of hydrothermal (Murray et al., 1991, 1992; Bau and Dulski, 1999; Franchi et al., 2015), (3) micro-sampling techniques were used to sample the limestones and avoid areas like muddy laminae, stylolites or fractures, and (4) 5% acetic acid is used for carbonate dissolution for the REY analyses to minimize the impact of terrigenous contamination (Webby and Kamber, 2000; Rongemaille et al., 2011).

3.2 Thin section observations

A total of twenty-five thin sections, as well as oriented and polished slabs, were cut perpendicular to bedding and were prepared at the China University of Geosciences (Beijing). Another set of thin sections were stained with Alizarin Red S to distinguish calcite and dolomite. The petrography, depositional structures, and diagenesis characteristics in these thin sections were described using a Leica polarizing microscope housed at the Bureau of Economic Geology, the University of Texas at Austin.

3.3 Geochemical analyses

All samples were crushed and powdered down to a grain-size smaller than 200-mesh for geochemical analyzes. A total of 500 mg powder was obtained for each sample.

Approximately 200 mg of powdered samples were analyzed for major and trace elements. Major elements were measured using an X-ray fluorescence spectrometer (AB-104L), with an analytical precision better than 2%. For trace elements, samples were cleaned in ultra-pure water before dissolution in 2 ml of 15 N double-distilled HNO_3. Solutions were then spiked with 10 ppb of internal standards for NexION300D ICP-MS (ELAN DRC-e) analyses with an analytical precision better than 5%. All geochemical tests were performed at the analytical laboratory of the Beijing Research Institute of Uranium Geology. The experimental procedures have been described in other publications (e.g., Nothdurft et al., 2004).

About 50 mg of powdered samples were weighted for the carbon and oxygen isotope analyses. These samples were reacted in an inert atmosphere with ultrapure concentrated (100%) orthophosphoric acid at 25ºC in a Thermo-Finnigan Gasbench II. The CO_2 from carbonate minerals was then automatically released through a chromatographic column and delivered via a stream of helium to the source of a Thermo Scientific MAT253 stable isotope mass spectrometer, where the gas was ionized, and its isotopic ratios were measured. All the reported values were based on the Vienna Pee Dee Belemnite (V-PDB) standard by referring to GBW-04416 (reference number GB04416: $\delta^{13}C = 1.61‰ \pm 0.03‰$ V-PDB, $\delta^{18}O = -11.59‰ \pm 0.11‰$ V-PDB). The test results are presented in ‰. The precisions of the $\delta^{18}O$ and $\delta^{13}C$ measurements are ±0.1‰ and ±0.2‰,

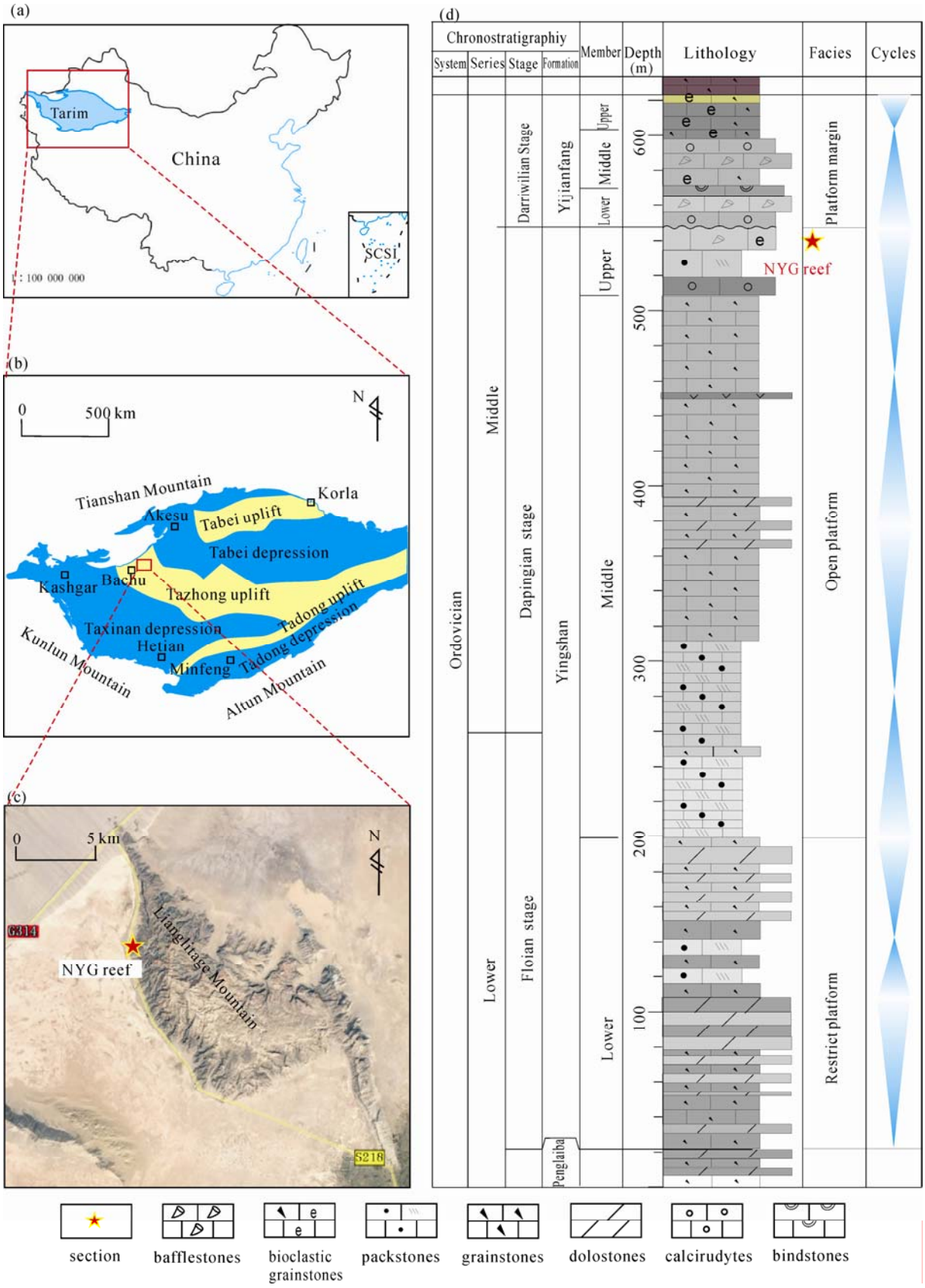

Fig. 1. Tectonic sketch map of the Tarim Basin and stratigraphic column of the Lower to Middle Ordovician.
(a) the location of the Tarim Basin in China (after China National Bureau of Surveying and Mapping Geographical Information); (b) the tectonic units of the Tarim Basin; (c) the location of the NYG reef along the Lianglitage Mountain; (d) the stratigraphic column of the Lower to Middle Ordovician at the Lianglitage Mountain (modified from Guo et al., 2010).

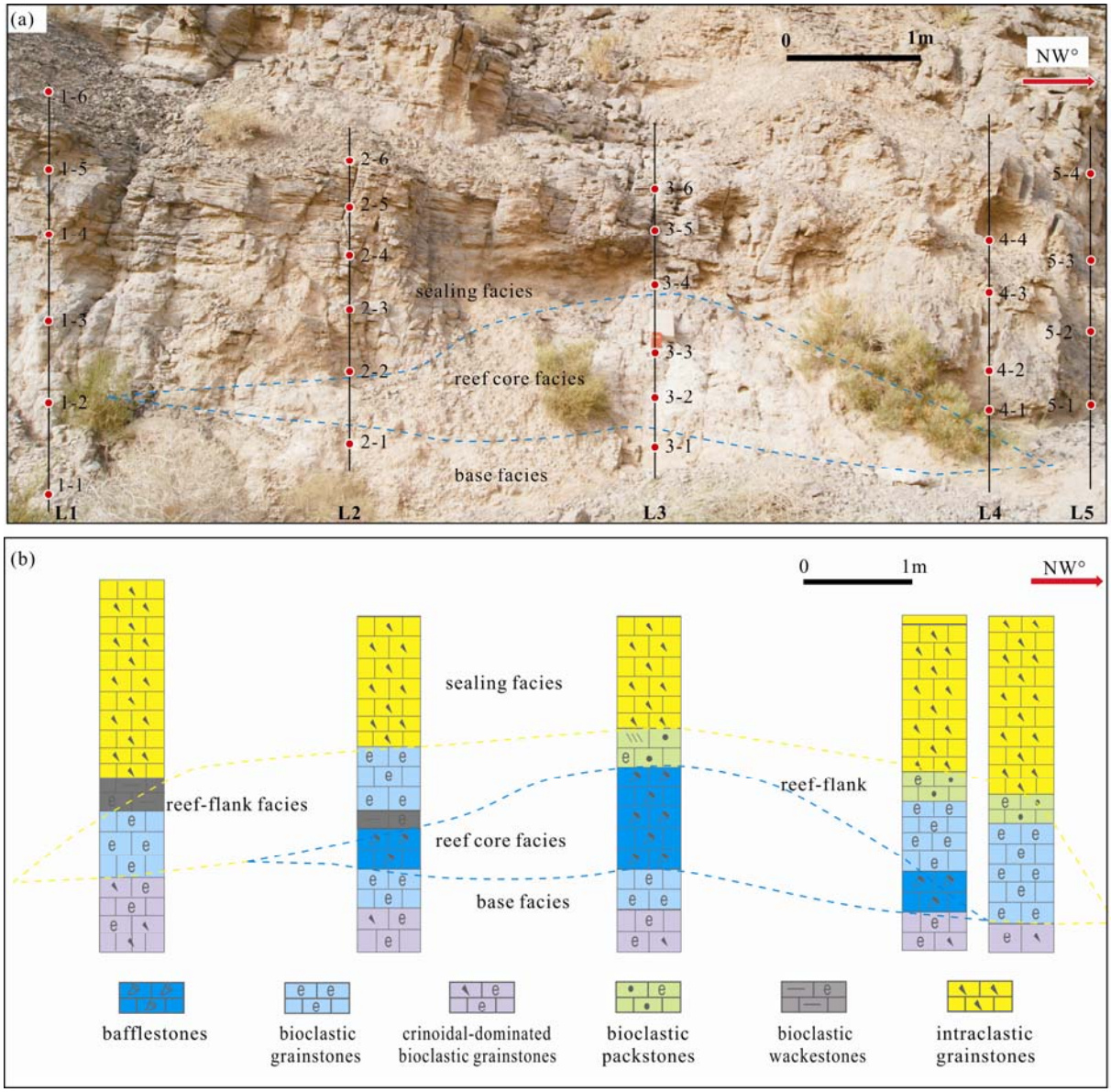

Fig. 2. Morphologies and sampling locations of the NYG reef.
(a) five vertical transects (L1-L5) (outlined by blue closed curves) and locations of samples (red dots) in the NYG reef; (b) facies units of the NYG reef, including the base facies, reef-core facies, reef-flank facies, and sealing facies.

respectively.

4 Results

4.1 Petrography and diagenesis

Based on the types of lithology and organisms, as well as the geometric characteristics, from bottom to top, the reef is subdivided into four depositional facies: the base facies, reef-core facies, reef-flank facies, and sealing facies (Fig. 1e), adopting the nomenclature proposed by Gül and Eren (2003). The base facies is mainly composed of bioclastic grainstones (Fig. 3a). The reef-core facies is the major part of the reef buildup and displays a low-relief dome. The main lithology in this subfacies is composed of bafflestones, and the reef-building organism is *Calathium* (Li et al., 2017b; Fig. 3b). The reef-flank facies deposits on top of the reef-core facies and is mainly composed of bioclastic wackestones and packstones (Fig. 3c). The predominant lithology of the sealing facies is intraclastic grainstones (Fig. 3d). Stratigraphically, this reef evolved from an initial colonization phase (base facies) into a vertical aggradation phase (reef-core facies) and ultimately into a capping phase (sealing facies), that is mainly controlled by sea-level changes (Meng et al., 2018).

The diagenetic fabrics include cements, dissolution pores and fractures which is linked to the following three main stages: marine, subaerial exposure and meteoric, and burial diagenesis. Marine (near-surface) diagenesis accompanied the deposition of micrite and micritic algae, skeletal components, and accretion of sediments. It is supported by the occurrence of the fibrous or bladed isopachous (C1) marine cements (Fig. 4a–d) with internal

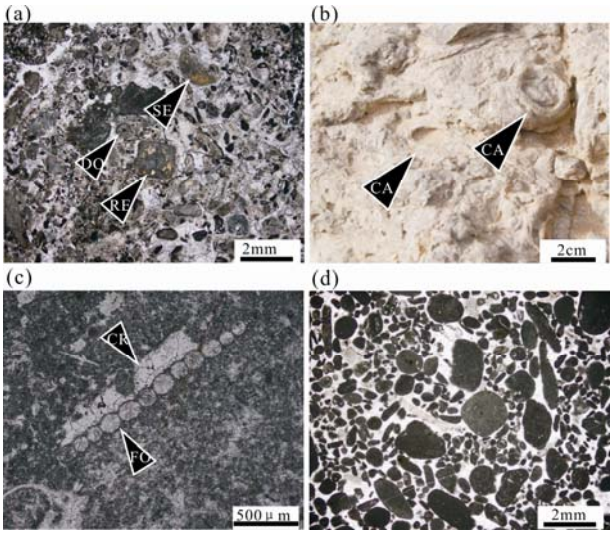

Fig. 3. Lithologies from different facies units of the NYG reef.
(a) photomicrograph shows bioclastic grainstones from the reef base, in which crinoids are the main bioclasts, which are shown as donut-shaped (DO), semicircular (SE), or rectangular (RE) (sample NYG-2-1, plane-polarized light); (b) bafflestones from the reef core, Calathium framworks (CA) are scattered in the reef core; (c) photomicrograph shows the bioclastic wackestones from the reef-flank, in which bioclasts contain single-row foraminifera (FO) and crinoid (CR) (sample NYG-1-3, plane-polarized light). (d) photomicrograph showing the intraclastic grainstones from the sealing facies, in which grains have a high degree of roundness (sample NYG-3-5, plane-polarized light).

sediments and microborings. Subaerial exposure and meteoric diagenesis resulted in the development of an early secondary dissolution pores (D1, D2) (Fig. 4a–c). Meteoric equant cements (C2) precipitated below water table in some of the interparticle pore spaces (Fig. 4a–d). Burial diagenesis accompanied exists of microfractures (Fig. 4e, 4f) that affected by the tectonic movement.

4.2 Geochemical results

4.2.1 Major and trace elements

Analyses of major elements indicate that the CaO contents of these samples (ranging from 50.58% to 56.23%, with an average of 54.38%) are close to the theoretical value of calcite (56.03%). Moreover, the total value of Al, Fe, K, Na, Ti, P, Mg, and Mn are all less than 5‰. This means that these samples represent pure limestones that are dominantly composed of calcite. The results of major and trace elements are listed in Tables 1 and 2.

4.2.2 Isotopes data

The $\delta^{18}C$ values of reefal limestones are clustered around zero (ranging from −0.70‰ to +0.60‰, with an average of 0), whereas the $\delta^{13}O$ values vary from −7.30‰ to −4.80‰, with an average of −6.00‰ (Table 2). A plot of all carbon and oxygen isotope data shows no apparent correlation between $\delta^{18}O$ and $\delta^{13}C$ values (Fig. 5).

4.2.3 Rare earth elements and Yttrium (REYs)

The REY concentrations of twenty-five samples are shown in Table 3. The REY contents in most plots are

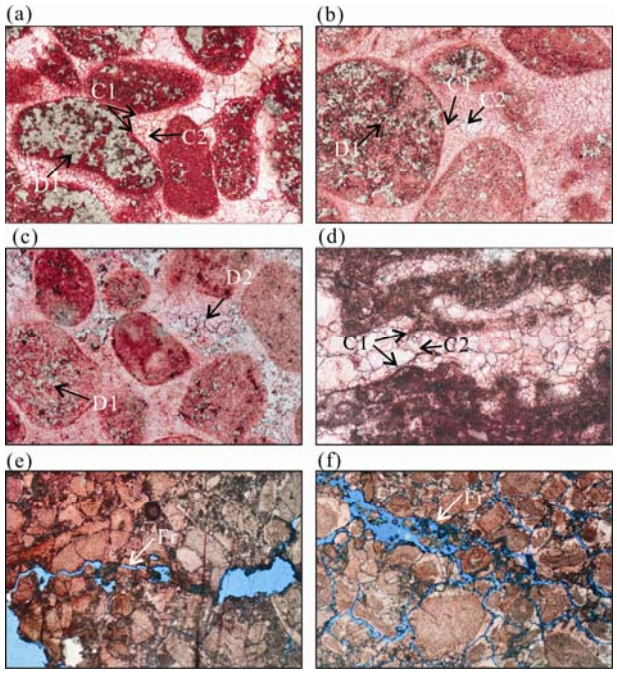

Fig. 4. The diagenetic features of the NYG reef.
(a) photomicrograph of intraclastic grainstones; arrows point at the fibrous isopachous cement (C1), early equant cement (C2) and intraparticle dissolution pore (D1) (sample NYG-3-6, plane-polarized light); (b) photomicrograph of intraclastic grainstones; arrows point at the fibrous isopachous cement (C1), early equant cement (C2) and intraparticle dissolution pore (D1) (sample NYG-5-4, plane-polarized light); (c) photomicrograph of intraclastic grainstones; arrows point at the intraparticle dissolution pore (D1) and interparticle dissolution pore (D2) (sample NYG-4-2, plane-polarized light); (d) photomicrograph of algae grainstones (sample 2-2); arrows point at the bladed isopachous cement (C1) and early equant cement (C2) (sample NYG-2-2, plane-polarized light); (e) photomicrograph of bioclastic grainstones; arrows point at the microfracture (Fr) (sample NYG-2-1, plane-polarized light); (f) photomicrograph of bioclastic grainstones; arrows point at the microfracture (Fr) (sample NYG-4-1, plane-polarized light).

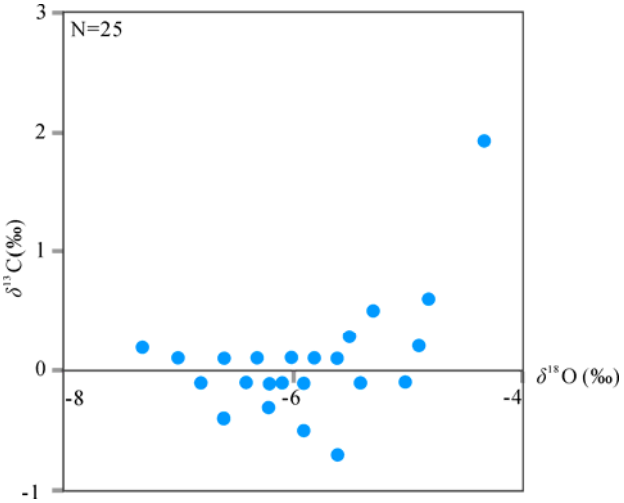

Fig. 5. Cross-plot of carbon and oxygen isotopes from twenty-five samples of the NYG reef.

normalized (and given the subscript SN) to a standard shale average (PAAS-Post Archaean Australian Shales;

Table 1 Major elements results of samples from the NYG reef (wt%)

Number	Samples	Lithologies	facies units	Ca	Si	Al	Fe	K	Na	Ti	P	Mg	Mn
1	NYG-1-1	Bioclasticic packstones	base facies	55.45	1.040	0.116	<0.010	0.021	0.148	0.008	0.007	0.302	<0.0031
2	NYG-1-2	Peloidal grainstones	base facies	56.23	0.540	0.110	<0.010	0.025	0.063	0.006	0.008	0.202	0.002
3	NYG-1-3	Bioclasticic wackestones	reef-flank facies	55.74	0.551	0.181	<0.010	0.036	0.052	0.007	0.006	0.275	<0.0031
4	NYG-1-4	Intraclasticic grainstones	sealing facies	55.13	1.150	0.300	<0.010	0.096	0.054	0.016	0.007	0.287	0.004
5	NYG-1-5	Intraclasticic grainstones	sealing facies	55.62	1.150	0.344	0.038	0.113	0.061	0.018	0.007	0.328	0.004
6	NYG-1-6	Intraclasticic grainstones	sealing facies	55.62	1.150	0.292	0.032	0.106	0.050	0.017	0.006	0.312	0.005
7	NYG-2-1	Bioclasticic packstones	reef base	55.66	0.658	0.119	0.011	0.031	0.050	0.007	0.006	0.227	0.002
8	NYG-2-2	Bioclasticic wackestones	reef-flank facies	55.73	0.849	0.138	<0.010	0.040	0.048	0.010	0.007	0.278	<0.0031
9	NYG-2-3	Peloidal grainstones	reef-flank facies	55.36	1.310	0.292	0.031	0.090	0.058	0.015	0.007	0.307	0.002
10	NYG-2-4	Intraclasticic grainstones	sealing facies	54.35	1.700	0.360	0.039	0.119	0.070	0.016	0.007	0.377	<0.0031
11	NYG-2-5	Intraclasticic grainstones	sealing facies	55.07	1.010	0.253	0.027	0.085	0.062	0.014	0.007	0.392	0.002
12	NYG-2-6	Intraclastic grainstones	sealing facies	54.28	1.870	0.460	0.092	0.162	0.057	0.025	0.006	0.373	0.006
13	NYG-3-1	Bioclastic wackestones	base facies	55.78	0.520	0.126	<0.010	0.035	0.065	0.009	0.007	0.233	0.002
14	NYG-3-2	Bafflestones	reef-core facies	55.73	0.921	0.135	<0.010	0.031	0.060	0.006	0.007	0.238	0.002
15	NYG-3-3	Bafflestones	reef-core facies	55.30	0.554	0.109	0.012	0.028	0.047	0.009	0.008	0.257	0.003
16	NYG-3-5	Intraclastic grainstones	sealing facies	54.03	1.780	0.385	0.141	0.138	0.084	0.023	0.009	0.309	0.004
17	NYG-3-6	Intraclastic grainstones	sealing facies	54.35	1.400	0.348	0.023	0.132	0.050	0.020	0.007	0.337	0.004
18	NYG-4-1	Bioclastic packstones	reef-flank facies	53.33	4.610	0.191	0.017	0.074	0.053	0.013	0.006	0.444	0.002
19	NYG-4-2	Intraclastic grainstones	sealing facies	53.96	2.840	0.236	0.033	0.087	0.082	0.013	0.006	0.471	<0.0031
20	NYG-4-3	Intraclastic grainstones	sealing facies	54.27	2.160	0.411	0.084	0.159	0.082	0.024	0.009	0.406	0.005
21	NYG-4-4	Intraclastic grainstones	sealing facies	53.63	2.090	0.500	0.096	0.167	0.104	0.024	0.007	0.385	0.004
22	NYG-5-1	Bioclastic grainstones	reef-flank facies	54.04	2.260	0.355	0.046	0.093	0.089	0.014	0.010	0.438	<0.0031
23	NYG-5-2	Intraclastic grainstones	sealing facies	54.39	2.060	0.412	0.058	0.174	0.083	0.028	0.008	0.428	0.005
24	NYG-5-3	Intraclastic grainstones	sealing facies	53.33	3.030	0.260	0.017	0.093	0.054	0.013	0.008	0.500	<0.0031
25	NYG-5-4	Intraclastic grainstones	sealing facies	54.72	1.680	0.441	0.110	0.125	0.112	0.015	0.008	0.371	0.003
		Minimum value		53.33	0.520	0.109	0.011	0.021	0.047	0.006	0.006	0.202	0.002
		Maximum value		56.23	4.610	0.500	0.141	0.174	0.148	0.028	0.010	0.500	0.006
		Average value		54.84	1.555	0.2750	0.050	0.090	0.070	0.015	0.007	0.339	0.004
		Standard deviation		0.85	0.951	0.124	0.038	0.049	0.024	0.006	0.001	0.081	0.001

Table 2 Trace elements and carbon and oxygen isotopes results of samples from the NYG reef

Number	Samples	V (ppm)	Cr (ppm)	Co (ppm)	Cu (ppm)	Zn (ppm)	Sr (ppm)	Mo (ppm)	Ba (ppm)	Th (ppm)	U (ppm)	Zr (ppm)	δ^{13}C (PDB) (‰)	δ^{18}O (PDB) (‰)
1	NYG-1-1	6.17	2.570	1.300	0.392	2.220	307.000	0.219	2.970	0.133	1.060	0.477	–0.40	–6.60
2	NYG-1-2	7.73	3.120	1.460	0.650	2.460	174.000	0.248	5.480	0.150	0.825	0.500	0.10	–6.60
3	NYG-1-3	7.01	2.440	1.330	0.419	1.990	238.000	0.204	9.060	0.183	0.773	0.703	0.10	–6.30
4	NYG-1-4	7.14	3.230	1.390	0.786	3.670	230.000	0.356	20.000	0.558	2.160	1.630	0.10	–6.60
5	NYG-1-5	6.84	3.390	1.440	0.892	3.340	290.000	0.313	32.100	0.640	1.800	1.950	–0.30	–6.20
6	NYG-1-6	6.98	3.290	1.590	1.070	3.490	286.000	0.333	43.600	0.593	1.790	1.910	–0.10	–6.10
7	NYG-2-1	5.38	2.250	1.530	0.991	3.230	213.000	0.307	4.780	0.194	0.734	0.533	0.10	–7.00
8	NYG-2-2	6.78	2.560	1.330	0.527	2.250	256.000	0.222	6.790	0.194	0.753	0.699	0.10	–6.30
9	NYG-2-3	6.91	3.350	1.310	0.875	3.550	224.000	0.461	18.300	0.510	2.210	1.340	–0.10	–6.20
10	NYG-2-4	7.82	3.950	1.410	0.681	6.100	352.000	0.367	9.400	0.606	1.370	1.880	–0.10	–5.40
11	NYG-2-5	6.54	3.000	1.400	0.604	2.550	322.000	0.416	10.700	0.425	1.420	1.270	–0.10	–5.00
12	NYG-2-6	6.75	4.270	1.860	0.867	5.650	291.000	0.614	21.300	0.844	1.620	2.630	0.10	–5.80
13	NYG-3-1	9.88	2.970	1.320	0.823	2.860	205.000	0.177	4.770	0.170	0.642	1.630	–0.10	–6.80
14	NYG-3-2	10.60	2.660	1.230	0.590	3.430	248.000	0.178	11.900	0.158	0.875	1.320	0.20	–7.30
15	NYG-3-3	9.88	2.990	1.260	0.781	2.900	277.000	0.331	18.600	0.184	1.300	0.820	0.10	–6.00
16	NYG-3-5	8.30	4.270	1.400	3.330	4.980	252.000	0.475	22.300	0.787	1.750	3.920	–0.50	–5.90
17	NYG-3-6	9.03	3.700	1.320	0.732	4.290	283.000	0.250	22.000	0.718	2.370	2.760	–0.10	–6.40
18	NYG-4-1	6.92	3.340	1.330	0.801	2.210	362.000	0.272	6.830	0.282	0.834	1.500	0.10	–5.80
19	NYG-4-2	8.66	2.960	1.230	1.120	2.860	409.000	0.361	7.930	0.354	0.571	2.060	0.30	–5.50
20	NYG-4-3	8.87	4.110	1.280	0.972	4.800	291.000	0.553	23.200	0.772	1.320	3.210	0.60	–4.80
21	NYG-4-4	9.07	4.290	1.480	3.280	4.340	280.000	0.549	38.800	0.928	1.700	3.870	–0.70	–5.60
22	NYG-5-1	8.47	5.720	1.580	217.00	4.130	327.000	0.536	10.900	0.478	1.830	3.010	–0.10	–5.90
23	NYG-5-2	9.04	4.710	1.400	1.230	4.380	294.000	0.305	13.500	0.822	1.640	3.750	0.10	–5.60
24	NYG-5-3	7.81	4.980	1.370	0.622	3.460	449.000	0.277	24.100	0.492	0.927	2.260	0.50	–5.30
25	NYG-5-4	9.85	3.650	2.710	0.599	4.930	336.000	1.390	16.900	0.518	1.700	2.790	0.20	–4.90
Minimum value		5.38	2.250	1.230	0.392	1.990	174.000	0.177	2.970	0.133	0.571	0.477	–0.70	–7.30
Maximum value		10.6	5.720	2.710	217.00	6.100	449.000	1.390	43.600	0.928	2.370	3.920	0.60	–4.80
Average value		7.94	3.511	1.450	9.625	3.603	287.840	0.389	16.248	0.468	1.359	1.937	0.00	–6.00
Standard deviation		1.35	0.856	0.296	43.209	1.118	62.961	0.243	10.655	0.256	0.534	1.076	0.28	0.65

McLennan, 1989). Yttrium (Y) has been inserted between Ho and Dy in analyses of REY patterns due to its similar properties to the Lanthanides and similar radius to its neighbors (Bau and Dulski, 1996).

The ratios of Nd_{SN}/Yb_{SN} are computed to determine the "depletion" of LREEs owning to the presence of positive La anomalies and negative Ce anomalies in shallow seawater (Nothdurft et al., 2004). The calculation of Ce and La anomalies follows the technique of Bau and Dulski (1996), where $Pr/Pr^* = Pr_{SN}/ (0.5\ Ce_{SN} + 0.5\ Nd_{SN})$ and

Table 3 The REY concentrations of 25 from the NYG reef (ppm)

Sample	NYG-1-1	NYG-1-2	NYG-2-1	NYG-3-1	NYG-3-2	NYG-3-3	NYG-1-3	NYG-2-2	NYG-2-3	NYG-4-1	NYG-5-1	NYG-1-4
Facies	Base	Base	Base	Base	Reef-core	Reef-core	Reef-flank	Reef-flank	Reef-flank	Reef-flank	Reef-flank	Sealing
La	0.762	0.809	1.120	0.702	0.602	0.673	0.806	0.777	2.490	0.990	1.260	2.860
Ce	1.240	1.280	1.790	1.160	0.954	1.130	1.310	1.260	4.160	1.770	2.140	5.100
Pr	0.134	0.141	0.202	0.142	0.120	0.118	0.154	0.136	0.458	0.207	0.254	0.565
Nd	0.506	0.513	0.721	0.553	0.481	0.440	0.505	0.539	1.650	0.763	1.000	2.160
Sm	0.087	0.079	0.110	0.092	0.095	0.089	0.098	0.079	0.258	0.129	0.194	0.364
Eu	0.017	0.018	0.024	0.016	0.017	0.018	0.024	0.018	0.055	0.026	0.034	0.067
Gd	0.064	0.084	0.100	0.095	0.095	0.097	0.105	0.087	0.239	0.142	0.159	0.344
Tb	0.014	0.012	0.018	0.021	0.018	0.015	0.017	0.018	0.039	0.021	0.037	0.056
Dy	0.062	0.077	0.100	0.116	0.121	0.083	0.098	0.083	0.221	0.129	0.191	0.322
Y	0.772	0.660	0.915	1.050	1.160	0.857	0.894	0.761	1.560	0.908	1.400	2.400
Ho	0.017	0.016	0.022	0.024	0.020	0.017	0.019	0.018	0.049	0.028	0.037	0.064
Er	0.049	0.052	0.074	0.087	0.067	0.065	0.064	0.058	0.151	0.084	0.118	0.204
Tm	0.010	0.008	0.011	0.014	0.013	0.011	0.012	0.012	0.023	0.014	0.019	0.034
Yb	0.054	0.046	0.076	0.081	0.083	0.071	0.081	0.068	0.157	0.098	0.122	0.203
Lu	0.008	0.007	0.010	0.011	0.015	0.010	0.011	0.010	0.022	0.012	0.021	0.025
ΣREY	3.796	3.802	5.293	4.164	3.861	3.694	4.198	3.924	11.532	5.321	6.986	14.768
Ce/Ce*	0.842	0.822	0.818	0.801	0.773	0.870	0.809	0.841	0.847	0.852	0.824	0.874
Eu/Eu*	1.060	1.023	1.066	0.794	0.831	0.896	1.095	1.003	1.032	0.888	0.903	0.882
Pr/Pr*	1.070	1.100	1.125	1.117	1.113	1.058	1.197	1.043	1.106	1.126	1.095	1.076
Gd/Gd*	0.787	1.184	0.961	0.853	0.951	1.128	1.086	0.911	1.035	1.168	0.775	1.043
Nd_{SN}/Yb_{SN}	0.820	0.976	0.830	0.597	0.507	0.542	0.546	0.694	0.920	0.681	0.717	0.931
Dy_{SN}/Yb_{SN}	0.731	1.065	0.837	0.911	0.928	0.744	0.770	0.777	0.896	0.838	0.996	1.009
Y/Y*	2.257	1.791	1.860	1.895	2.220	2.172	1.969	1.877	1.429	1.440	1.583	1.590
Y/Ho	45.412	41.250	41.591	43.750	58.000	50.412	47.053	42.278	31.837	32.429	37.838	37.500

Sample	NYG-1-5	NYG-1-6	NYG-2-4	NYG-2-5	NYG-2-6	NYG-3-5	NYG-3-6	NYG-4-2	NYG-4-3	NYG-4-4	NYG-5-2	NYG-5-3	NYG-5-4
Facies	Sealing	Sealing	Sealing	Sealing	Sealing	Sealing	Sealing	Sealing	Sealing	Sealing	Sealing	Sealing	Sealing
La	2.620	3.850	1.740	2.320	3.380	2.680	2.490	1.600	2.880	3.000	2.590	1.710	1.990
Ce	4.710	7.040	3.170	3.950	6.320	4.810	4.710	2.910	5.320	5.580	4.720	3.150	3.600
Pr	0.543	0.757	0.377	0.447	0.741	0.561	0.531	0.338	0.607	0.648	0.546	0.363	0.427
Nd	2.040	2.760	1.430	1.610	2.820	2.170	2.090	1.300	2.360	2.590	2.110	1.380	1.600
Sm	0.384	0.473	0.261	0.276	0.541	0.391	0.392	0.232	0.490	0.490	0.402	0.254	0.274
Eu	0.074	0.085	0.041	0.047	0.090	0.073	0.072	0.041	0.080	0.082	0.075	0.054	0.053
Gd	0.364	0.473	0.224	0.257	0.482	0.441	0.381	0.236	0.472	0.437	0.392	0.253	0.294
Tb	0.063	0.076	0.042	0.047	0.089	0.075	0.068	0.041	0.085	0.084	0.071	0.043	0.050
Dy	0.358	0.420	0.225	0.217	0.506	0.401	0.418	0.243	0.492	0.490	0.411	0.245	0.312
Y	2.380	2.960	1.510	1.680	3.240	2.700	2.620	1.630	2.850	2.960	2.780	2.040	2.220
Ho	0.073	0.090	0.048	0.051	0.114	0.090	0.079	0.051	0.097	0.098	0.083	0.057	0.064
Er	0.208	0.258	0.143	0.142	0.293	0.234	0.235	0.139	0.289	0.307	0.232	0.169	0.180
Tm	0.039	0.050	0.021	0.023	0.054	0.046	0.043	0.027	0.045	0.054	0.040	0.029	0.033
Yb	0.224	0.272	0.151	0.152	0.305	0.274	0.250	0.167	0.311	0.317	0.244	0.169	0.205
Lu	0.032	0.037	0.018	0.020	0.044	0.038	0.036	0.021	0.045	0.047	0.038	0.025	0.029
ΣREY	14.112	19.601	9.401	11.239	19.019	14.984	14.415	8.976	16.423	17.184	14.734	9.941	11.331
Ce/Ce*	0.861	0.898	0.853	0.845	0.870	0.855	0.893	0.862	0.877	0.872	0.865	0.871	0.851
Eu/Eu*	0.921	0.835	0.791	0.822	0.822	0.811	0.867	0.813	0.774	0.826	0.879	0.990	0.864
Pr/Pr*	1.107	1.086	1.118	1.121	1.108	1.096	1.069	1.097	1.082	1.075	1.093	1.100	1.124
Gd/Gd*	1.000	1.071	0.918	0.957	0.938	1.063	0.985	1.018	0.977	0.912	0.976	1.028	1.049
Nd_{SN}/Yb_{SN}	0.797	0.888	0.829	0.927	0.809	0.693	0.732	0.681	0.664	0.715	0.757	0.714	0.683
Dy_{SN}/Yb_{SN}	1.017	0.983	0.948	0.908	1.056	0.931	1.064	0.926	1.007	0.984	1.072	0.923	0.969
Y/Y*	1.402	1.451	1.385	1.522	1.286	1.355	1.369	1.395	1.241	1.285	1.433	1.646	1.496
Y/Ho	32.603	32.889	31.458	32.941	28.421	30.000	33.165	31.961	29.381	30.204	33.494	35.789	34.688

$Ce/Ce^*=Ce_{SN}/(0.5\,La_{SN}+0.5\,Pr_{SN})$. When Pr/Pr* >1.05, a negative Ce anomaly exists; when Ce/Ce* <1, a positive La anomaly exists. Gd_{SN} and Eu_{SN} anomalies were calculated as Gd_{SN}/Gd^* where Gd* = (0.5Eu + 0.5Tb) and as Eu/Eu* where $Eu^* = Eu_{SN}/(0.5Sm_{SN}+0.5Gd_{SN})$ (Bau and Dulski, 1996; Nothdurft et al., 2004). Y anomalies were calculated as Y_{SN}/Y^* where $Y^* = (0.5\,Dy_{SN}+0.5\,Ho_{SN})$ (Bau et al., 1996).

(1) The overall characteristic of REY patterns

The REY concentrations of reefal limestones in the study area are generally low (ranging from 2.7 ppm to 22.0 ppm, arithmetic mean 9.2 ppm). The REYs of all samples have flat patterns, but also exhibit subtle variations. When comparing the REYs to that of modern seawater, the total REYs (ΣREYs) are generally three to four orders of magnitude higher in concentration. With the increase of REY concentrations, changes can be discerned from seawater-like to shale-like patterns (Fig. 6). Reefal limestones in this study have relatively low ΣREYs than that of modern carbonates.

All samples show the seawater-like REE_{SN} distributions: characteristic of light REE (LREE) depletion

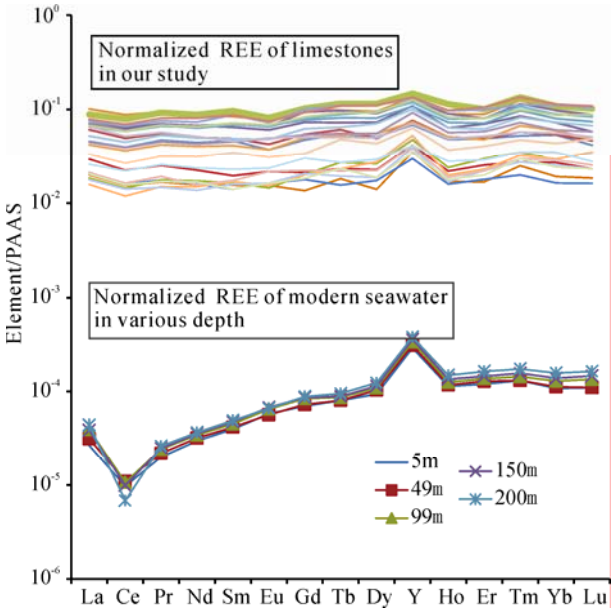

Fig. 6. Mean PAAS-normalized REY patterns of different facies of the NYG reef, as shown in table 3. PAAS-normalized REY patterns of modern seawater from different water depths are also displayed for comparison (Alibo and Nozaki, 1999).

(Nd_{SN}/Yb_{SN} range from 0.51 to 0.98, average at 0.75) (Table 3; Fig. 6), positive Pr_{SN} anomalies (Pr/Pr* range from 1.04 to 1.20, average at 1.10) and negative Ce_{SN} anomalies (Ce/Ce* range from 0.77 to 0.90, average at 0.85) (Fig. 7), and positive Y anomalies (Y_{SN}/Y^* range from 1.24 to 2.26, average at 1.62) (Table 3).

Gd_{SN} anomalies are in the range of 0.78 to 1.18, with an average of 0.99. Twelve out of twenty-five samples have slightly positive Gd anomalies. The Y/Ho ratios of samples range from 28.4 to 58.0, with an average of 37.5. To explore the effect of facies on REY characteristics, we further differentiate these REYs specific to each facies.

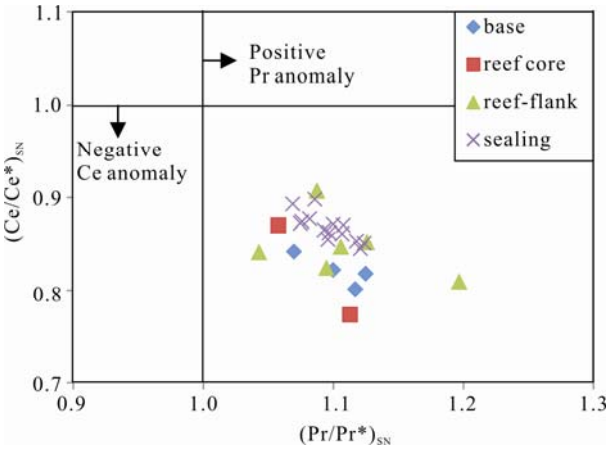

Fig. 7. Cross-plot shows the relationship between Ce/Ce* and Pr/Pr* using the method described by Bau and Dulski (1996) (as modified by Webb and Kamber, 2000).
Note that nearly all samples cluster tightly in the field of negative Ce and positive La anomalies in perfect agreement with modern open oceanic surface water.

(2) REY patterns in each facies

The REY concentrations in different facies are shown in Table 4 and Fig. 8. Samples from the reef-core facies show the lowest values of total REY (ΣREY), light REE (LREE), medium REE (MREE), and heavy REE (HREE) (3.78 ppm, 2.35 ppm, 1.24 ppm and 0.19 ppm, respectively). In contrast, samples from the sealing facies display the highest values of ΣREE, LREE, MREE, and HREE (14.01ppm, 10.14 ppm, 3.28 ppm and 0.60 ppm, respectively). Samples from both the base facies and reef-flank facies have REE values that are slightly higher than the reef-core facies but significantly lower than the sealing facies.

Samples from the base facies (n=4) show seawater-like REY patterns (Fig. 8a) with the characteristics of (1) LREE depletion (average Nd_{SN}/Yb_{SN}=0.81, SD=0.16), (2) slightly negative Ce and positive La anomalies (mean Ce/Ce*=0.82 and mean Pr/Pr*=1.10), (3) slightly high Y/Ho ratios (mean 43.0, SD=1.95), and (4) weak negative Gd

Table 4 Summary statistics of REY concentrations (ppm) of the four facies in the NYG reef

	Base (n=4)				Reef-core (n=2)				Reef-flank (n=5)				Sealing (n=14)			
	Min	Max	Ave	SD	Min	Max	Ave	SD	Min	Max	Ave	SD	Min	Max	Ave	SD
La	0.702	1.120	0.848	0.186	0.602	0.673	0.638	0.050	0.777	2.490	1.265	0.712	1.600	3.850	2.551	0.647
Ce	1.160	1.790	1.368	0.286	0.954	1.130	1.042	0.124	1.260	4.160	2.128	1.192	2.910	7.040	4.649	1.213
Pr	0.134	0.202	0.155	0.032	0.118	0.120	0.119	0.001	0.136	0.458	0.242	0.129	0.338	0.757	0.532	0.131
Nd	0.506	0.721	0.573	0.101	0.440	0.481	0.461	0.029	0.505	1.650	0.891	0.468	1.300	2.820	2.030	0.504
Sm	0.079	0.110	0.092	0.013	0.089	0.095	0.092	0.004	0.079	0.258	0.152	0.074	0.232	0.541	0.373	0.101
Eu	0.016	0.024	0.019	0.004	0.017	0.018	0.018	0.001	0.018	0.055	0.031	0.014	0.041	0.090	0.067	0.016
Gd	0.064	0.100	0.086	0.016	0.095	0.097	0.096	0.001	0.087	0.239	0.146	0.059	0.224	0.482	0.361	0.094
Tb	0.012	0.021	0.016	0.004	0.015	0.018	0.017	0.002	0.017	0.039	0.026	0.011	0.041	0.089	0.064	0.017
Dy	0.062	0.116	0.089	0.024	0.083	0.121	0.102	0.027	0.083	0.221	0.144	0.060	0.217	0.506	0.361	0.102
Y	0.660	1.050	0.849	0.170	0.857	1.160	1.009	0.214	0.761	1.560	1.105	0.352	1.510	3.240	2.426	0.546
Ho	0.016	0.024	0.020	0.004	0.017	0.020	0.019	0.002	0.018	0.049	0.030	0.013	0.048	0.114	0.076	0.021
Er	0.049	0.087	0.066	0.018	0.065	0.067	0.066	0.001	0.058	0.151	0.095	0.039	0.139	0.307	0.217	0.057
Tm	0.008	0.014	0.011	0.003	0.011	0.013	0.012	0.001	0.012	0.023	0.016	0.005	0.021	0.054	0.038	0.011
Yb	0.046	0.081	0.064	0.017	0.071	0.083	0.077	0.008	0.068	0.157	0.105	0.035	0.151	0.317	0.232	0.059
Lu	0.007	0.011	0.009	0.002	0.010	0.015	0.013	0.004	0.010	0.022	0.015	0.006	0.018	0.047	0.033	0.010
ΣREYs	3.796	5.293	4.264	0.707	3.694	3.861	3.778	0.118	3.924	11.532	6.392	3.115	8.976	19.601	14.009	3.425
LREE	2.649	3.943	3.036	0.609	2.252	2.450	2.351	0.140	2.791	9.016	4.677	2.566	6.380	14.880	10.135	2.577
MREE	0.851	1.298	1.059	0.206	1.070	1.411	1.241	0.241	0.967	2.114	1.453	0.490	2.042	4.407	3.279	0.768
HREE	0.129	0.217	0.169	0.043	0.174	0.198	0.186	0.017	0.166	0.402	0.262	0.098	0.381	0.823	0.595	0.156

Note: n= total sample numbers

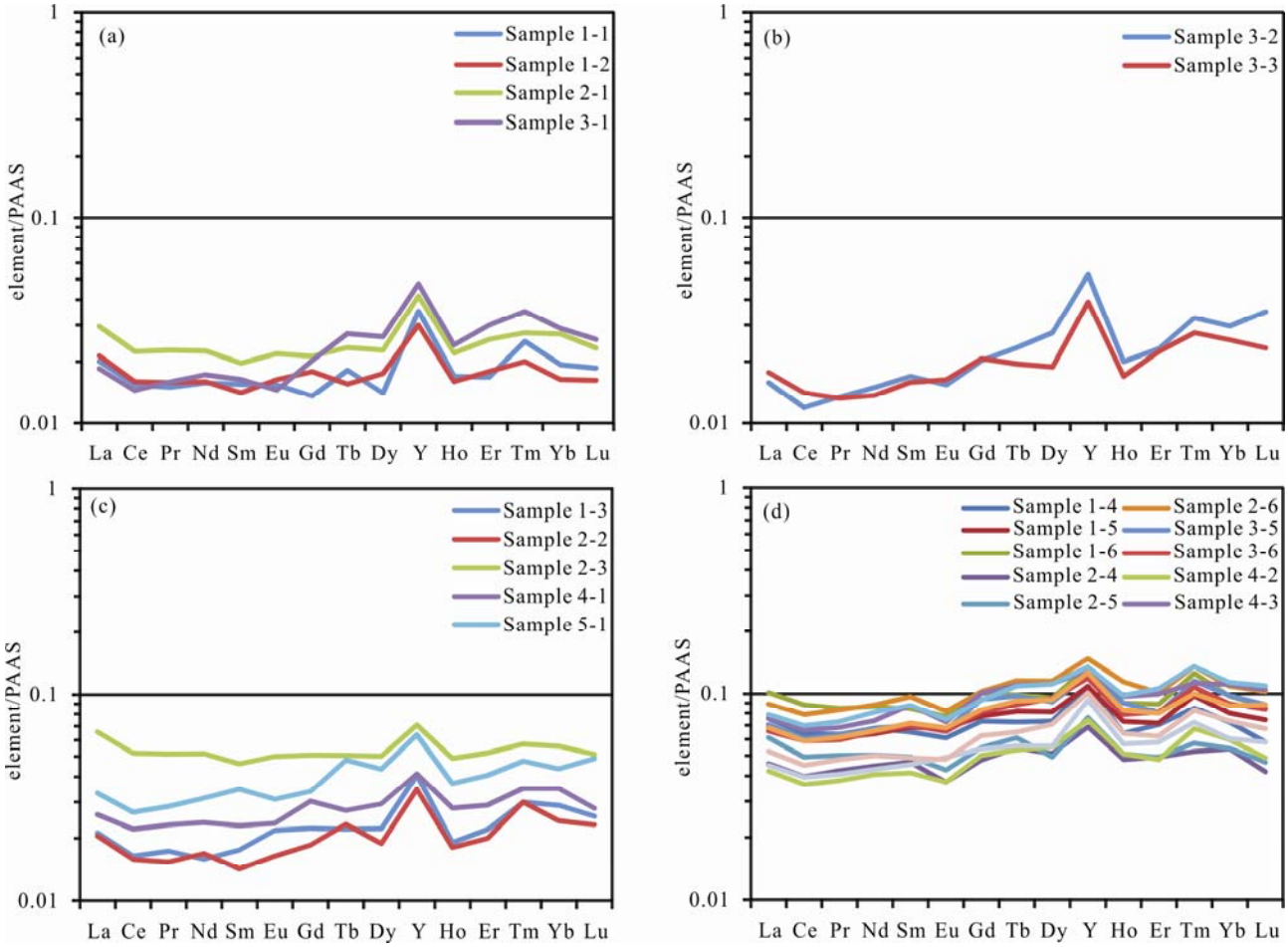

Fig. 8. Shale-normalized REY patterns of different facies of the NYG reef.
(a) REE patterns of samples from the base facies (n=4); (b) REE patterns of samples from the reef-core facies (n=2); (c) REE patterns of samples from the reef-flank facies (n=5); (d) REE patterns of samples from the sealing facies (n=10).

anomalies (mean Gd/Gd*=0.95).

Samples from the reef-core facies (n=2) have seawater-like REY patterns (Fig. 8b) with the characteristics of (1) LREE depletion (mean Nd_{SN}/Yb_{SN}=0.56, SD=0.02), (2) consistent negative Ce and weak positive La anomalies (mean Ce/Ce*=0.81 and mean Pr/Pr*=1.09), (3) relatively high Y/Ho ratios (mean 54.2, SD=5.37), and (4) consistently weak positive Gd anomalies (mean Gd_{SN}/Gd*=1.04).

Samples from the reef-flank facies (n=5) show less seawater-like features (Fig. 8c). However, LREE depletions (mean Nd_{SN}/Yb_{SN}=0.71, SD=0.13), and negative Ce anomalies and positive La anomalies (mean Ce/Ce*=0.84 and mean Pr/Pr*=0.02) are present. It also shows non-seawater-like features (1) weakly negative Gd anomalies (mean Gd/Gd*=1.00), and (2) low Y/Ho ratios (mean 38.3, SD=6.5).

Samples from the sealing facies (n=14) display non-seawater-like characteristics including their REY patterns (Fig. 8d), low Y/Ho ratios (mean 32.5, SD=2.5), and lack of Gd anomalies (mean Gd/Gd*=1.00). However, LREE depletion (mean Nd_{SN}/Yb_{SN}=0.77, SD=0.09), negative Ce and positive La anomalies (mean Ce/Ce*=0.88 and mean Pr/Pr*=1.10) are observed in these samples as well.

5 Discussion

5.1 Implication for carbon and oxygen Isotopes

The original geochemical signals of ancient marine carbonates can be easily modified by diagenetic processes such as meteoric water diagenesis, sulfate reduction and dolomitization (Jiang et al., 2018a, 2018b). These processes can change the primary chemical composition of the seawater at the time of deposition (Veizer and Hoefs, 1976; Veizer et al., 1999). Thus, it is essential to evaluate the potential diagenetic alteration impacts.

A compilation of C and O isotopes of carbonates is widely used to study the origin and the nature of diagenetic fluids (Jiang et al., 2018a, 2018b). For example, the most-positive $\delta^{18}O$ value of Paleozoic marine limestones likely represent the original precipitation conditions with the least diagenetic alterations (Tobin and Bergstrom, 2002; Trotter et al., 2008). Hence, mudstones from the Ordovician strata of the Tarim Basin yield the more positive $\delta^{18}O$ values than dolomites and veins, which likely retain the original ancient seawater information (Fig. 9; Zhang et al., 2006; Liu et al., 2016). The $\delta^{13}C$ values of limestone samples in this study vary from −0.9‰ to +0.9‰ but cluster around zero, and the $\delta^{18}O$

values varies from approximately −7‰ to −5‰, which shows relatively positive C and O isotopes values. This means that limestone samples are clearly not modified by diagenesis (Trotter et al., 2008; Saltzman and Thomas, 2012)

5.2 Sources of REY patterns

The processes that can affect REY concentrations and patterns in carbonates include diagenesis (German and Elderfield, 1990; Byrne et al., 1996; Azmy et al., 2011, 2013; Li and Jones, 2014; Jiang et al., 2015), unusual redox conditions (Bau et al., 1996; Webb and Kamber, 2000), and terrestrial detritus (Goldstein and Jaconsen, 1988; Elderfield et al., 1990; Nothdurft et al., 2004; Frimmel, 2009). To assess the potential factors that control the sources of REYs, factor analysis followed by multiple linear regressions with REY is performed. This analysis minimizes the impact of co-linearity of the variable regression models.

5.2.1 Diagenesis effects

Ancient carbonates have commonly been considered unreliable sources for REY proxies, owing to perceived problems with diagenetic alterations (e.g., Holser, 1997), Elements, such as Ba, Na, Sr, Mg, and P, have been utilized as indicators of the susceptibility of a rock to diagenetic alteration of the REY patterns (Li and Jones, 2013a, 2013b; Li and Jones, 2014). To assess whether diagenesis controls the REY distributions, we examined the relationship between the REYs and these elements. Univariate analysis indicated the weak correlation between these elements and REY contents (Table 5). Although phosphates have a high affinity for ΣREYs in diagenetic fluids and show non-uniform incorporation across the REY mass range in some cases (German and Elderfield, 1990; Byrne et al., 1996), the very low P concentrations and its irrelevance to the ΣREYs (Fig. 10) suggest that the diagenesis did not change the REE concentrations.

Further, weak negative Eu anomalies (range from 0.77 to 1.10, mean 0.90) present in these reefal carbonates has precluded diagenetic processes such as hydrothermal events and thermochemical sulfate reduction. These processes typically cause a prominent positive Eu anomaly (Banner et al., 1988; Michard, 1989; Murray et

Table 5 Correlation coefficients of the relationship between diagenesis-related elements and Σ REYs of the NYG reef

	ΣREYs	Ba	Na	Sr	Mg	P
ΣREYs	1					
Ba	0.674	1				
Na	0.048	−0.095	1			
Sr	0.097	0.138	0.197	1		
Mg	0.360	0.190	0.227	0.873	1	
P	−0.080	0.170	0.257	0.112	0.174	1

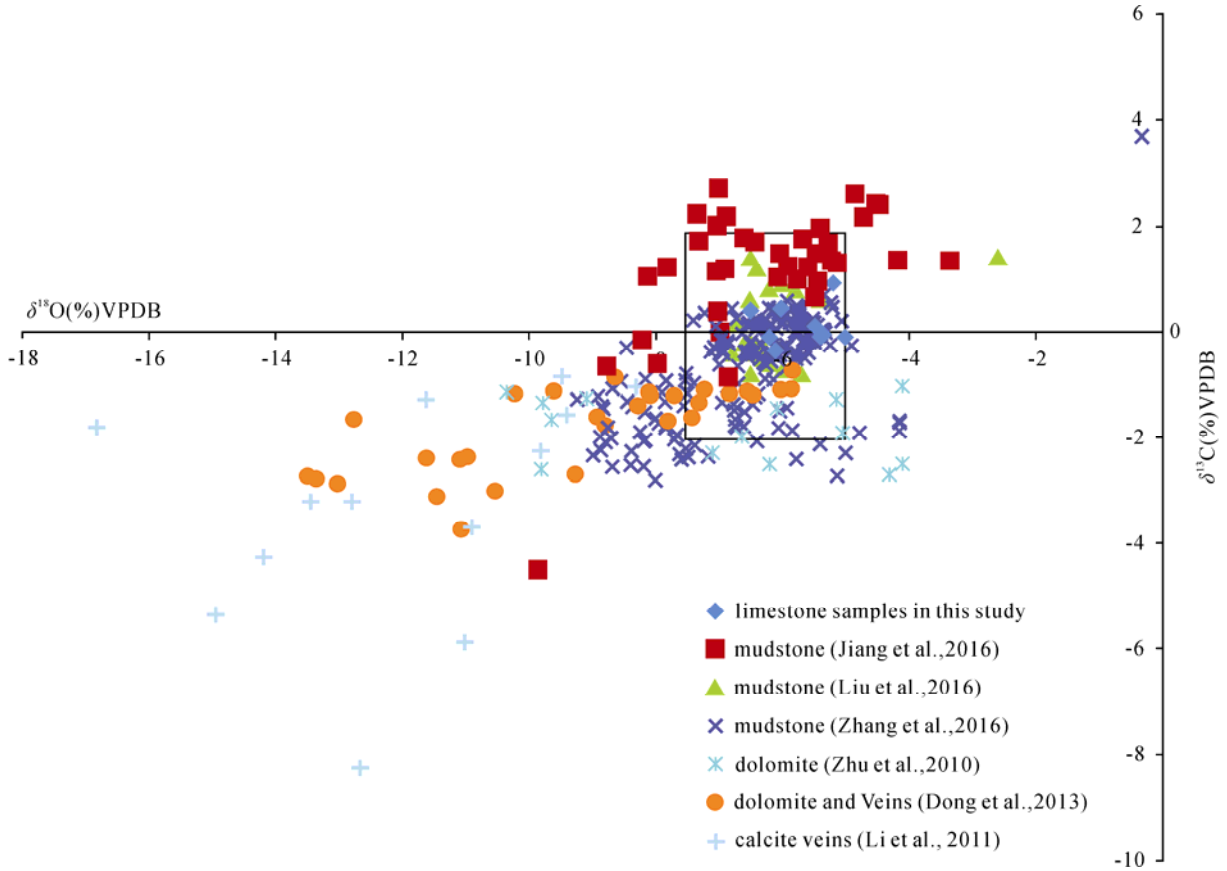

Fig. 9. Summary of C and O isotopes from the Ordovician strata of the Tarim basin. Data of mudstones, dolomites, and calcite veins is collected from previous papers (Jiang et al., 2001; Zhang et al., 2006; Zhu et al., 2010; Li et al., 2011; Dong et al., 2013; Liu et al., 2016). The rectangle shows the ranges of C and O isotopes from conodonts and brachiopods through Ordovician (data from Trotter et al., 2008; Saltzman and Thomas, 2012).

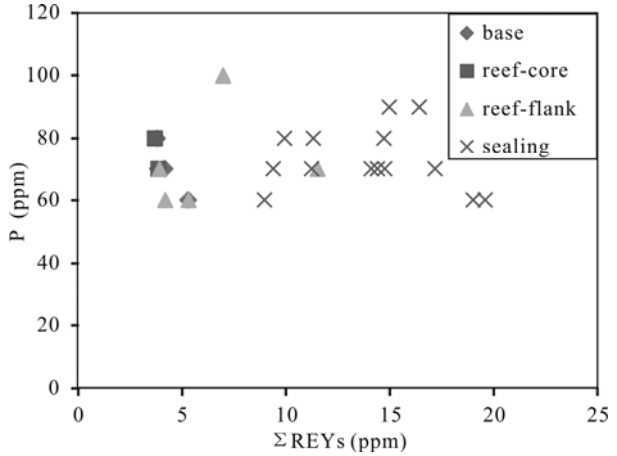

Fig. 10. The scatter plot shows phosphates vs ΣREYs of samples from the NYG reef, where P concentrations that do not correlate with ΣREEs, suggesting that diagenesis does not alter REY concentrations.

al., 1991).

5.2.2 Redox conditions

Elements, such as Co, Cr, Cu, V, Fe, U, Zn, and Mo, are redox-sensitive (Algeo and Maynard, 2004; Eltom, et al., 2017). Accordingly, the correlation coefficients between redox-sensitive trace elements and ΣREYs of the NYG reef were computed to test whether changes in redox conditions have altered REY distributions (Table 6). The results show that these elements are poorly correlated with the total REYs. This means that REY distributions are unlikely altered by the change of redox conditions.

5.2.3 Terrestrial input

The REY concentrations in marine carbonates are very sensitive to terrestrial detritus. Small amounts of detrital contaminants can significantly change the total REY contents and patterns of carbonates (Nothdurft et al., 2004; Frimmel, 2009).

Elements, such as Zr, Th, and Al, have been demonstrated to be useful indictors for evaluating the extent of contamination from terrestrial detritus (Nothdurft et al., 2004; Frimmel, 2009; Eltom et al., 2017). These elements have high concentrations in detrital minerals but very low abundances in seawater. As depicted in Fig. 11, there is a positive correlation between the total REY concentrations and contents of Zr, Th, and Al. This likely indicates the contamination of mud (shale). The samples from both the sealing facies and reef-flank facies have high REY contents and low Y/Ho values, and they are likely contaminated by terrestrial detritus.

Another approach to evaluate detrital siliciclastic influences is based on Y/Ho ratios, which differ between sediments with detrital sources (about 25–30) and hydrogenous sources (about 60) (Webb and Kamber, 2000; Mclennan, 2001). This study shows that the mean Y/Ho ratios of the reef-core facies (54.206, SD = 5.366) are in the range of shallow seawater (44–76). Specifically, the mean Y/Ho ratios of the base facies (43.0) are close to those expected for shallow seawater. Whereas the mean Y/Ho ratios of the reef-flank facies and sealing facies are 38.3 and 32.5, respectively (Table 7, Fig. 12), which are lower than the values of shallow seawater. The low Y/Ho ratios of the reef-flank facies and sealing facies are consistent with the introduction of terrestrial detritus. This detritus may represent the accumulation of windblown dust in these facies. In this case, the extent of Y/Ho will likely be related to the water energy level of the sedimentary environment

Table 6 Correlation coefficients of the relationship between redox-sensitive trace elements and ΣREYs of the NYG reef

	ΣREYs	Co	Cr	Cu	V	Fe	U	Zn	Mo
ΣREYs	1.00								
Co	0.28	1.00							
Cr	0.51	0.22	1.00						
Cu	−0.10	0.10	0.54	1.00					
V	−0.08	0.05	0.22	0.07	1.00				
Fe	0.64	0.52	0.55	0.06	0.20	1.00			
U	0.69	0.25	0.46	0.19	0.03	0.41	1.00		
Zn	0.64	0.42	0.64	0.11	0.25	0.72	0.54	1.00	
Mo	0.35	0.87	0.33	0.13	0.23	0.69	0.37	0.53	1.00

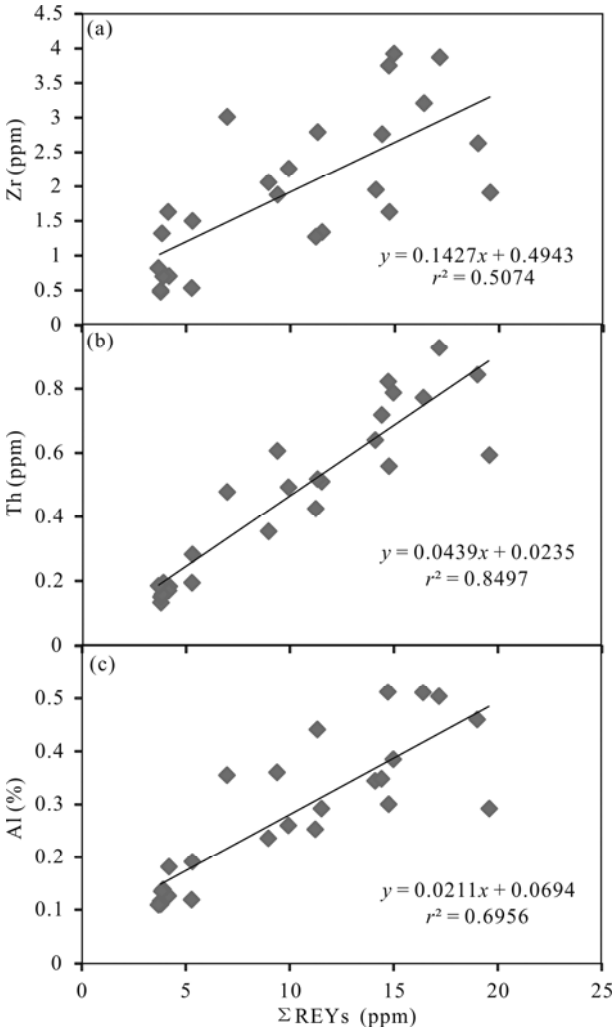

Fig. 11. Plot shows that positive correlations between REY concentrations and Zr, Th and Al, reflecting that the reefal limestones are easily affected by terrestrial contaminations.

Table 7 Comparisons of mean ratiosof Nd_{SN}/Yb_{SN}, Y/Ho,Pr/Pr*, Ce/Ce*, Gd/Gd* and ΣREYs of different facies

Facies	LREE depletion (Nd_{SN}/Yb_{SN})		Y/Ho		Pr/Pr*		Ce/Ce*		Gd/Gd*		ΣREYs (ppm)	
	Ave	SD	Ave	SD	Ave	SD	Ave	SD	Ave	SD	Ave	n
Base	0.806	0.156	43.001	1.952	1.103	0.024	0.819	0.012	0.946	0.174	4.264	4
Reef-core	0.525	0.018	54.206	5.366	1.086	0.039	0.814	0.068	1.039	0.125	3.778	2
Reef-flank	0.711	0.134	38.287	6.498	1.113	0.056	0.843	0.023	0.995	0.154	6.392	5
Sealing	0.773	0.092	32.464	2.506	1.097	0.018	0.880	0.014	0.995	0.052	14.009	14

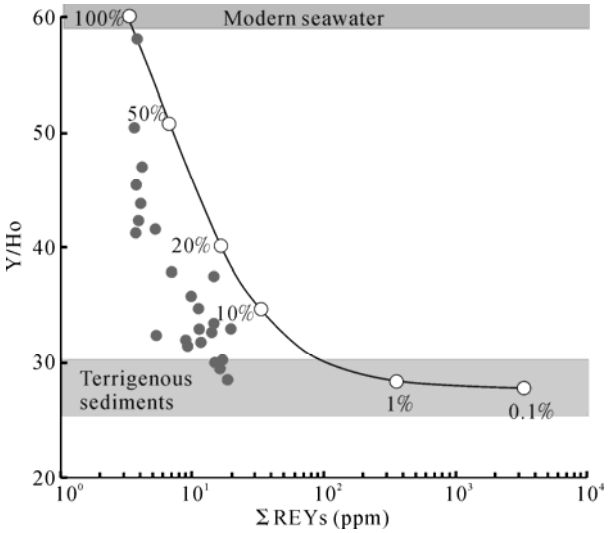

Fig. 12. Y/Ho versus ΣREYs for reefal limestones samples from the NYG reef.

The gray area represents the Y/Ho percentages of terrigenous component with UCC composition (McLennan, 2001); the percentage curve is given as amount of the hydrogenous component (Nozaki, 2001).

where these rocks accumulated.

5.3. Potential for REY proxies of reefal limestones to paleoenvironment study

The REY data presented above have shown that the reefal limestones have a dominantly seawater-like character, although there are exceptions to this generalization. After analyzing the relationship between REYs and the sensitive elements, we conclude that diagenesis and redox condition have no or weak effects while terrestrial detritus have a significant effect on the REY patterns.

The relative low Y/Ho ratios and high REY concentrations in the reef-flank and sealing facies appear to reflect the impact of terrestrial detritus input. The REY characteristics of reef-flank facies and sealing facies therefore cannot be used to estimate the composition of Ordovician ancient seawater of the Tarim Basin. However, REY patterns of base facies and reef-core facies may have potential in preserving the contemporaneous seawater signals. Increasing in the input of terrestrial detritus into shelf reef facies can be driven by a decreased sea-level, resulting in an increased erosion rate (Grötsch, 2009; Jiao et al., 2012).

6 Conclusions

The most significant findings of this study on the REY characteristics of reefal limestones in the Ordovician Tarim Basin are as follows:

(1) Diagenesis has little effect on the REY patterns of reefal limestones, hence these REY patterns can be used to study the paleoenvironment.

(2) The REY contents of reefal limestones are low (range from 3.69 to 19.60 ppm, mean 10.22 ppm). The PAAS-normalized REY patterns of all samples generally show consistent and flat patterns and display seawater-like features. However, REY partitioning behaviors are also related to facies: the base facies and reef-core facies are characterized by seawater-like features, whereas, the reef-flank facies and sealing facies contain both seawater-like and non-seawater-like features.

(3) Both negative Nd_{SN}/Yb_{SN} anomalies (ranging from 0.51 to 0.98) and values of Dy_{SN}/Yb_{SN} anomalies (ranging from 0.73 to 1.07) are consistent with the observation of LREE depletion. Positive La anomalies, negative Ce anomalies, and positive Y anomalies suggest that these reefal limestones are likely an indicative of contemporaneous seawater REY signals.

(4) The low Y/Ho ratios (range from 28.42 to 58.00, mean 37.51) of the samples from the reef-flank facies and sealing facies suggest non-seawater-like characteristics. These low Y/Ho ratios and non-seawater-like characteristics are most likely impacted by terrestrial detritus. Hence, this study confirms that depositional environments can be a controlling factor when applying REY to the study of marine paleoenvironment.

Acknowledgements

This research is supported by the National Natural Science Foundation of China (grant number 51574208), the National 973 Program of China (grant number 2012CB214802), and the China Geological Survery Project (grant number DD20190217). Miaomiao Meng would like to acknowledge the China Scholar Council (grant number 201606400023) for providing the financial support when studying at the University of Texas at Austin. We also thank the anonymous reviewers for their insightful comments which helped improve the manuscript.

Manuscript received Aug. 1, 2018
accepted Dec. 20, 2018
associate EIC ZHANG Hongfu
edited by LIU Lian

References

Algeo, T.J., and Maynard, J.B., 2004. Trace-element behavior and redox facies in core shales of Upper Pennsylvanian Kansas-type cyclothems. Chemical Geology, 206(3): 289–318.

Alibo, D.S., and Nozaki, Y., 1999. Rare earth elements in

seawater: particle association, shale-normalization, and Ce oxidation. Geochimica et Cosmochimica Acta, 63(3): 363–372.
Allwood, A.C., Kamber, B.S., Walter, M.R., Burch, I.W., and Kanik, I., 2010. Trace elements record depositional history of an Early Archean stromatolitic carbonate platform. Chemical Geology, 270(1): 148–163.
Allwood, A.C., Walter, M.R., Burch, I.W., and Kamber, B.S., 2007. 3.43 billion-year-old stromatolite reef from the Pilbara Craton of Western Australia: ecosystem-scale insights to early life on Earth. Precambrian Research, 158(3-4): 198–227.
Azmy, K., Brand, U., Sylvester, P., Gleeson, S. A., Logan, A., and Bitner, M. A., 2011. Biogenic and abiogenic low-Mg calcite (bLMC and aLMC): Evaluation of seawater-REE composition, water masses and carbonate diagenesis. Chemical Geology, 280(1): 180–190.
Azmy, K., Lavoie, D., Wang, Z., Brand, U., Al-Aasm, I., Jackson, S., and Girard, I., 2013. Magnesium-isotope and REE compositions of Lower Ordovician carbonates from eastern Laurentia: implications for the origin of dolomites and limestones. Chemical Geology, 356: 64–75.
Banner, J.L., Hanson, G.N., Meyers, and W.J., 1988. Rare earth element and Nd isotopic variations in regionally extensive dolomites from the Burlington-Keokuk Formation (Mississippian): Implications for REE mobility during carbonate diagenesis. Journal of Sedimentary Research, 58(3): 415–432.
Bau, M., 1996. Controls on the fractionation of isovalent trace elements in magmatic and aqueous systems: evidence from Y/Ho, Zr/Hf, and lanthanide tetrad effect. Contributions to Mineralogy and Petrology, 123(3): 323–333.
Bau, M., and Dulski, P., 1996. Distribution of yttrium and rare-earth elements in the Penge and Kuruman iron-formations, Transvaal Supergroup, South Africa. Precambrian Research, 79(1-2): 37–55.
Bau, M., and Dulski, P., 1999. Comparing yttrium and rare earths in hydrothermal fluids from the Mid-Atlantic Ridge: implications for Y and REE behavior during near-vent mixing and for the Y/Ho ratio of Proterozoic seawater. Chemical Geology, 155(1): 77–90.
Bau, M., Koschinsky, A., Dulski, P., and Hein, J.R., 1996. Comparison of the partitioning behaviors of yttrium, rare earth elements, and titanium between hydrogenetic marine ferromanganese crusts and seawater. Geochimica et Cosmochimica Acta, 60(10): 1709–1725.
Byrne, R.H., Liu, X., and Schijf, J., 1996. The influence of phosphate coprecipitation on rare earth distributions in natural waters. Geochimica et Cosmochimica Acta, 60(17): 3341–3346.
Cai, C.F., Li, K.K., Li, H., and Zhang, B., 2008. Evidence for cross formational hot brine flow from integrated Sr/Sr, REE and fluid inclusions of the Ordovician veins in Central Tarim, China. Applied Geochemistry, 23(8): 2226–2235.
Dong, S., Chen, D., Qing, H., Zhou, X., Wang, D., Guo, Z., Jiang, M., and Qian, Y., 2013. Hydrothermal alteration of dolostones in the lower Ordovician, Tarim Basin, NW China: multiple constraints from petrology, isotope geochemistry and fluid inclusion microthermometry. Marine & Petroleum Geology, 46(3): 270–286.
Elderfield, H., Upstill-Goddard, R., and Sholkovitz, E.R., 1990. The rare earth elements in rivers, estuaries, and coastal seas and their significance to the composition of ocean waters. Geochimica et Cosmochimica Acta, 54(4): 971–991.
Elderfield, H., Whitfield, M., Burton, J.D., Bacon, M.P., and Liss, P.S., 1988. The oceanic chemistry of the rare-earth elements. Philosophical Transactions of the Royal Society of London. Series A, Mathematical and Physical Sciences, 105–126.
Eltom, H.A., Abdullatif, O.M., Makkawi, M.H., and Eltoum, I.E.A., 2017. Rare earth element geochemistry of shallow carbonate outcropping strata in Saudi Arabia: Application for depositional environments prediction. Sedimentary Geology, 348: 51–68.
Feng, D., Chen, D., and Peckmann, J., 2009. Rare earth elements in seep carbonates as tracers of variable redox conditions at ancient hydrocarbon seeps. Terra Nova, 21: 49–56.
Franchi, F., Hofmann, A., Cavalazzi, B., Wilson, A., and Barbieri, R., 2015. Differentiating marine vs hydrothermal processes in Devonian carbonate mounds using rare earth elements (Kess Kess mounds, Anti-Atlas, Morocco). Chemical Geology, 409: 69–86.
Frimmel, H.E., 2009. Trace element distribution in Neoproterozoic carbonates as palaeoenvironmental indicator. Chemical Geology, 258(3): 338–353.
German, C.R., and Elderfield, H., 1990. Application of the Ce anomaly as a paleoredox indicator: the ground rules. Paleoceanography, 5(5): 823–833.
Goldstein, S.J., and Jacobsen, S.B., 1988. Rare earth elements in river waters. Earth and Planetary Science Letters, 89(1): 35–47.
Greaves, M.J., Elderfield, H., and Sholkovitz, E.R., 1999. Aeolian sources of rare earth elements to the Western Pacific Ocean. Marine Chemistry, 68(1): 31–38.
Grötsch, J., 2009. Guilds, cycles and episodic vertical aggradation of a reef (late Barremian to early Aptian, Dinaric carbonate platform, Slovenia). Orbital Forcing and Cyclic Sequences (Special Publication 19 of the IAS), 38: 227.
Gu, J.Y., Zhang, X.Y., Luo, P., Luo, Z., and Fan, H., 2005. Development characteristics of organic reef-bank complex on Ordovician carbonate platform margin in Tarim Basin. Oil & Gas Geology, 26(3): 277–283 (In Chinese with English abstract).
Gül, M., and Eren, M., 2003. The sedimentary characteristics of Dagpazari patch reef (Middle Miocene, mut-içel/Turkey). Carbonates and Evaporites, 18(1): 51–62.
Guo, C.T., Li, R.Y., and Chen, S.M., 2018. Rare earth element geochemistry and genetic model of dolomite of Yingshan formation in Gucheng area, Tarim Basin. Journal of Jilin University (Earth Science Edition), 48(4): 1121–1134 (In Chinese with English abstract).
Guo, F., Lai, S.H., and Guo, L., 2010. Ordovician sequence stratigraphy and sedimentology in the Dabantage Area, Tarim Basin. Journal of Stratigraphy, 34(2): 135–144.
Han, Y.X., Zhong, L.I., and Han, D.L., 2009. REE characteristics of matrix dolomites and its origin of Lower Ordovidan in eastern Tabei area, Tarim Basin. Acta Petrologica Sinica, 25 (10): 2405–2416.
Holser, W.T., 1997. Evaluation of the application of rare-earth elements to paleoceanography. Palaeogeography, Palaeoclimatology, Palaeoecology, 132(1): 309–323.
Hu, Y., Feng, D., Peckmann, J., Roberts, H.H., and Chen, D., 2014. New insights into cerium anomalies and mechanisms of trace metal enrichment in authigenic carbonate from hydrocarbon seeps. Chemical Geology, 381: 55–66.
Huang, B., Zhu, R., Otofuji, Y.A., and Yang, Z., 2000. The Early Paleozoic paleogeography of the North China block and the other major blocks of China. Chinese Science Bulletin, 45 (12): 1057–1065.
Huang, C.J., Liu, G.Y., Ma, Y.S., Liu, B., Liu, H.G., and Shi, K.B., 2017. New Insights into the Depositional Environments of Ordovician Carbonate Formations in the Yubei Area of Tarim Basin Based on Standard Microfacies Types. Acta Geologica Sinica (English Edition), 91(2): 755–756.
Jiang, L., Cai, C.F., Worden, R.H., Li, K.K., Xiang, L., Chu, X., and Li, W., 2015. Rare earth element and yttrium (REY) geochemistry in carbonate reservoirs during deep burial diagenesis: Implications for REY mobility during thermochemical sulfate reduction. Chemical Geology, 415: 87–101.
Jiang, L., Richard H. Worden, Cai, C.F., Li, K.K., Xiang, L., Cai, L.L., and He, X.Y., 2014. Dolomitization of gas reservoirs: the Upper Permian Changxing Formation and Lower Triassic Feixianguan Formation, Northeast Sichuan Basin, China. Journal of Sedimentary Research, 84: 792–815.
Jiang, L., Worden, R., and Yang, C.B., 2018. Thermochemical sulfate reduction can improve carbonate petroleum reservoir quality. Geochimica et Cosmochimica Acta, 223: 127–140.
Jiang, L., Worden, R., Cai C.F., Shen A.J., He, X.Y., and Pan, L.Y., 2018. Contrasting diagenetic evolution patterns of platform margin dolostone and limestone in the Lower

Triassic Feixianguan Formation, Sichuan Basin, China. Marine and Petroleum Geology, 92: 332–351.
Jiang, M.S., Zhu, J.Q., Chen, D.Z., Zhang, R.H., and Qiao, G.S., 2001. Carbon and strontium isotope variations and responses to sea-level fluctuations in the Ordovician of the Tarim Basin. Science China (Series D), 44(9): 816.
Jiao, Y.Q., Wu, L.Q., Rong, H., Wang, Y.B., and Wang, R., 2012. Paleoecology of the Ordovician reef-shoal depositional system in the Yijianfang outcrop of the Bachu Area, West Tarim Basin. Journal of Earth Science, 23(4): 408–420.
Kamber, B.S., and Webb, G.E., 2001. The geochemistry of late Archaean microbial carbonate: implications for ocean chemistry and continental erosion history. Geochimica et Cosmochimica Acta, 65(15): 2509–2525.
Kamber, B.S., Bolhar, R., and Webb, G.E., 2004. Geochemistry of late Archaean stromatolites from Zimbabwe; evidence for microbial life in restricted epicontinental seas. Precambrian Research, 132: 379–399.
Kang, Y.Z., and Kang, Z.H., 1996. Tectonic evolution and oil and gas of Tarim Basin. Journal of Southeast Asian Earth Sciences, 13(3): 317–325.
Kemp, R.A., and Trueman, C.N., 2003. Rare earth elements in Solnhofen biogenic apatite: geochemical clues to the palaeoenvironment. Sedimentary Geology, 155(1): 109–127.
Kim, J.H., Torres, M.E., Haley, B.A., Kastner, M., Pohlman, J.W., Riedel, M., and Lee, Y.J., 2012. The effect of diagenesis and fluid migration on rare earth element distribution in pore fluids of the northern Cascadia accretionary margin. Chemical Geology, 291: 152–165.
Li, K., Cai, C., He, H., Jiang, L., Cai, L., Xiang, L., Huang, S., and Zhang, C., 2011. Origin of palaeo-waters in the Ordovician carbonates in Tahe Oilfield, Tarim Basin: constraints from fluid inclusions and Sr, C and O isotopes. Geofluids, 11(1): 71–86.
Li, Q., Li, Y., and Kiessling, W., 2017a. The oldest labechiid stromatoporoids from intraskeletal crypts in lithistid sponge–Calathium reefs. Lethaia, 50(1): 140–148.
Li, Q., Li, Y., Zhang, Y., and Munnecke, A., 2017b. Dissecting Calathium-microbial frameworks: The significance of calathids for the Middle Ordovician reefs in the Tarim Basin, northwestern China. Palaeogeography, Palaeoclimatology, Palaeoecology, 474: 66–78.
Li, R., and Jones, B., 2013a. Heterogeneous diagenetic patterns in the Pleistocene Ironshore Formation of Grand Cayman, British West Indies. Sedimentary Geology, 294: 251–265.
Li, R., and Jones, B., 2013b. Temporal and spatial variations in the diagenetic fabrics and stable isotopes of Pleistocene corals from the Ironshore Formation of Grand Cayman, British West Indies. Sedimentary Geology, 286: 58–72.
Li, R., and Jones, B., 2014. Evaluation of carbonate diagenesis: A comparative study of minor elements, trace elements, and rare-earth elements (REE+Y) between Pleistocene corals and matrices from Grand Cayman, British West Indies. Sedimentary Geology, 314: 31–46.
Liu, C., Zhang, Y.J., Li, H.H., Cao, Y.H., Zhou, B., and Yang, M., 2017. Nature of Dolomitizing fluids of Middle-lower Ordovician dolomites in the Gucheng area, Tarim basin: Evidence from rare earth elements geochemistry. Bulletin of Mineralogy, Petrology and Geochemistry, 36(4): 602–610 (in Chinese with English abstract).
Liu, W., Huang, Q.Y., Wang, K., and Shi, S.Y., 2016. Dolomization and influence on reservoir development in deep -burial stage: a case study of lower Paleozoic in Tarim Basin. Natural Gas Geoscience, 27(5), 772–779 (in Chinese with English abstract).
McLennan, S.M., 1989. Rare earth elements in sedimentary rocks: influence of provenance and sedimentary processes. Geochemistry and Mineralogy of Rare Earth Elements, 169–200.
McLennan, S.M., 2001. Relationships between the trace element composition of sedimentary rocks and upper continental crust. Geochemistry, Geophysics, Geosystems, 2(4): 1–24.
Meng, M.M., Fan, T.L., Wei, D., and Wang, S.S., 2018. Sedimentary characteristics and reef-forming models of Ordovician reefs in the Lianglitage Area, NW Tarim Basin. Journal of Palaeogeography, 20(2): 175–189 (in Chinese with English abstract).
Michard, A., 1989. Rare earth element systematics in hydrothermal fluids. Geochimica et Cosmochimica Acta, 53 (3): 745–750.
Murray, R.W., Brink, M.R.B.T., Gerlach, D.C., Russ, G.P., and Jones, D.L., 1992. Interoceanic variation in the rare earth, major, and trace element depositional chemistry of chert: perspectives gained from the DSDP and ODP record. Geochimica et Cosmochimica Acta, 56(5): 1897–1913.
Murray, R.W., Ten Brink, M.R.B., Gerlach, D.C., Russ, G.P., and Jones, D.L., 1991. Rare earth, major, and trace elements in chert from the Franciscan Complex and Monterey Group, California: Assessing REE sources to fine-grained marine sediments. Geochimica et Cosmochimica Acta, 55(7): 1875–1895.
Nothdurft, L.D., Webb, G.E., and Kamber, B.S., 2004. Rare earth element geochemistry of Late Devonian reefal carbonates, Canning Basin, Western Australia: confirmation of a seawater REE proxy in ancient limestones. Geochimica et Cosmochimica Acta, 68: 263–283.
Piepgras, D.J., and Jacobsen, S.B., 1992. The behavior of rare earth elements in seawater: Precise determination of variations in the North Pacific water column. Geochimica et Cosmochimica Acta, 56(5): 1851–1862.
Rongemaille, E., Bayon, G., Pierre, C., Bollinger, C., Chu, N.C., Fouquet, Y., Riboulot, V., and Voisset, M., 2011. Rare earth elements in cold seep carbonates from the Niger delta. Chemical Geology, 286(3): 196–206.
Saltzman, M.R., and Thomas, E., 2012. Carbon isotope stratigraphy. The geologic time scale, 1: 207–232.
Shields, G.A., and Webb, G.E., 2004. Has the REE composition of seawater changed over geological time?. Chemical Geology, 204(1–2): 103–107.
Tobin, K.J., and Bergstrom, S.M., 2002. Implications of ordovician (≈460 myr) marine cement for constraining seawater temperature and atmospheric pCO_2. Palaeogeography Palaeoclimatology Palaeoecology,181(4): 399–417.
Torsvik, T.H., and Cocks, L.R.M., 2013. Gondwana from top to base in space and time. Gondwana Research, 24(3–4): 999–1030.
Trotter, J.A., Williams, I.S., Barnes, C.R., Lécuyer, C., and Nicoll, R.S., 2008. Did cooling oceans trigger Ordovician biodiversification? Evidence from conodont thermometry. Science, 321(5888): 550–554.
Veizer, J., Ala, D., Azmy, K., Bruckschen, P., Buhl, D., Bruhn, F., and Jasper, T., 1999. $^{87}Sr/^{86}Sr$, $\delta^{13}C$ and $\delta^{18}O$ evolution of Phanerozoic seawater. Chemical Geology, 161(1): 59–88.
Veizer, J., and Hoefs, J., 1976. The nature of $^{18}O/^{16}O$ and $^{13}C/^{12}C$ secular trends in sedimentary carbonate rocks. Geochimica et Cosmochimica Acta, 40(11): 1387–1395.
Wang, X.L., Jin, Z.J., Hu, W.X., Zhang, J.T., Qian, Y.X., Zhu, J.Q., and Li, Q., 2009. Using in situ REE analysis to study the origin and diagenesis of dolomite of Lower Paleozoic, Tarim Basin. Science in China, 52(5): 681–693.
Webb, G.E., and Kamber, B.S., 2000. Rare earth elements in Holocene reefal microbialites: a new shallow seawater proxy. Geochimica et Cosmochimica Acta, 64(9): 1557–1565.
Webby, B.D., 2002. Patterns of Ordovician reef development. SEPM Special Publication, 72: 129–179.
Yang, X., Li, H.L., Zhang, Z.P., Chen, Q.L., Chen, Y., and Xiong, P., 2017. Evolution of Neoproterozoic Tarim Basin in Northwestern China and Tectonic Background of the Lower Cambrian Hydrocarbon Source Rocks. Acta Geologica Sinica, 91(8): 21–28 (in Chinese with English abstract).
Zhang, W., Guan, P., Jian, X., Feng, F., and Zhou, C., 2014. In situ\r, geochemistry of Lower Paleozoic dolomites in the northwestern Tarim basin: Implications for the nature, origin, and evolution of diagenetic fluids. Geochemistry, Geophysics, Geosystems, 15(7): 2744–2764.
Zhang, X.F., Hu, W.X., Jin, Z.J., Zhang, J.T., Qian, Y.X., Zhu, J.Q., Zhu, D.Y., Wang, X.L., and Xie, X.M., 2008. REE compositions of Lower Ordovician dolomites in Central and

North Tarim Basin, NW China: A potential REE proxy for ancient seawater. Acta Geologica Sinica (English Edition), 82 (3): 610–621.

Zhang, X.F., Hu, W.X., Jin, Z.J., Zhang, J.T., Qian, Y.X., Zhu, J.Q., Zhu, D.Y., Wang, X.L., and Xie, X.M., 2010. REE Compositions of Lower Ordovician Dolomites in Central and North Tarim Basin, NW China: A Potential REE Proxy for Ancient Seawater. Acta Geologica Sinica (English Edition), 82(3): 610–621.

Zhang, X.F., Hu, W.X., Jin, Z.J., Zhu, D.Y., Zhang, J.T., and Wang, X.L., 2006. REE variation and implication of ordovician dolomites from Tarim Basin, nw china. Geochimica et Cosmochimica Acta, 70(18): A737–A737.

Zhu, D., Jin, Z., and Hu, W., 2010. Hydrothermal recrystallization of the Lower Ordovician dolomite and its significance to reservoir in northern Tarim Basin. Science China (Series D), 53(3): 368–381.

About the first author

MENG Miaomiao, female, born in 1988 in Dengzhou City, Henan Province; PhD; graduated from China University of Geosciences (Beijing); Researcher at the Guangzhou Marine Geological Survey, China Geological Survey. Recently, she focuses on marine geology and petroleum geology, including sedimentology, geochemistry and natural gas hydrate geology. E-mail: 18811309981@126.com; phone: +8618811309981.

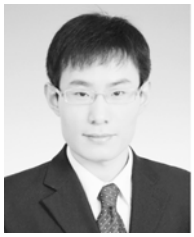

About the corresponding author

LIU Xinxing, male, born in 1987 in Xinxiang city, Henan province; PhD; graduated from China University of Geosciences (Beijing) since 2016. Lecturer at Hebei GEO University at present. He is now interested in mineral resource evaluation and remote sensing prospecting.